Natural Hazards Research 5 (2025) 175–186

Contents lists available at ScienceDirect

Natural Hazards Research

journal homepage: www.keaipublishing.com/en/journals/natural-hazards-research

A Convolutional Neural Network-based approach for automatically detecting rainfall-induced shallow landslides in a data-sparse context

Roquia Salam [a,b,*], Filiberto Pla [b,1], Bayes Ahmed [a,1], Marco Painho [c]

[a] Department of Risk and Disaster Reduction (RDR), University College London (UCL), Gower Street, London, WC1E 6BT, UK
[b] Institute of New Imaging Technologies, Universitat Jaume I (UJI), Castellón de la Plana, 12006, Spain
[c] NOVA Information Management School (NOVA IMS), Universidade Nova de Lisboa (UNL), Campus de Campolide, Lisbon, 1070-312, Portugal

ARTICLE INFO

Keywords:
Rainfall-induced shallow landslides
Data-sparse context
PlanetScope imagery
Sentinel-2 imagery
U-net model
Repeated stratified hold-out validation
Bangladesh

ABSTRACT

Detecting rainfall-induced shallow landslides in data-sparse regions has become increasingly important for effective landslides disaster management. Previous studies have predominantly focused on automated methods for deep-seated, earthquake-triggered landslides. This study addresses this gap by employing a U-net Convolutional Neural Network (CNN) model to detect rainfall-induced shallow landslides using multi-temporal, high-resolution PlanetScope (3m spatial resolution), medium-resolution Sentinel-2 (10m spatial resolution) imagery, and ALOS-PALSAR-provided digital elevation model (DEM). Four datasets were created: Datasets A and B using PlanetScope, and Datasets C and D using Sentinel-2, with Datasets B and D also including DEM data. A total of 181 manually delineated landslide polygons were used as ground truth masks. Each dataset was tested using repeated stratified hold-out validation. Performance metrics included precision, recall, F1 score, loss, and accuracy. Results indicated that Datasets A and B outperformed the others; however, integrating DEM with Dataset B did not enhance model accuracy. The best mean precision, recall, F1 score, loss, and accuracy were 1, 0.625, 0.625, 0.380, and 0.999, respectively, for both Datasets A and B. This study demonstrates the U-net model's potential for detecting rainfall-induced shallow landslides in various geographic and temporal contexts globally.

1. Introduction

All over the world, a significant number of extreme landslides occur in the rainy season in mountainous areas (Kumar et al., 2017). These rainfall-induced landslides are recurrent and catastrophic disasters, with long-lasting impacts on people's lives, livelihoods, critical infrastructure, and sustainable development (Mondini et al., 2023; Amatya et al., 2022). These dynamic events are influenced by natural factors like topography, geology, soil composition, and climate. Furthermore, climate change has a profound negative impact, leading to more frequent and severe rainfall-induced landslides (Das and Wegmann, 2022). Therefore, it is essential to properly understand the mechanisms that drive landslides to reduce the associated risks (Casagli et al., 2023). To minimize the risks of landslide disasters, it is crucial to have a comprehensive disaster management plan (Thirugnanam et al., 2020).

Landslide inventories are the primary resource for formulating a comprehensive landslide disaster management plan (CLDMP). Without them, it is impossible to conduct landslide risk and hazard assessments, susceptibility mapping, land use planning, and sustainable infrastructure development, all of which are key components of CLDMP. However, the process of creating landslide inventories varies worldwide. Some countries, such as Italy, the USA, Poland, Austria, and Norway, have strong, dedicated teams or groups within specific departments and recognized institutions that focus solely on creating or collecting landslide inventories (Karimi et al., 2019; Herrera et al., 2018). In these regions, the characteristics of landslides (mostly earthquake-triggered, dry, larger size deep-seated landslides) make them easier to identify through satellite images or field visits, even a long after the event. These developed countries usually have sufficient resources to create inventories. As a result, landslide inventory data can be collected from these dedicated departments and used to implement CLDMP. On the other hand, some countries or regions lack proper institutional mechanisms for collecting or creating landslide inventories, even though they are recognized as landslide-prone. These include Bangladesh, Myanmar, India, New Zealand, Rwanda, Ethiopia, Uganda, the Democratic Republic of the Congo, Burundi, and others (Meena et al., 2023; Rabby and Li, 2019; Monsieurs

* Corresponding author. Department of Risk and Disaster Reduction (RDR), University College London (UCL), Gower Street, London, WC1E 6BT, UK
E-mail addresses: roquia.salam.22@ucl.ac.uk (R. Salam), pla@uji.es (F. Pla), bayes.ahmed@ucl.ac.uk (B. Ahmed), painho@novaims.unl.pt (M. Painho).
[1] These authors contributed equally to this work.

https://doi.org/10.1016/j.nhres.2024.09.001
Received 14 August 2024; Received in revised form 22 September 2024; Accepted 22 September 2024
Available online 24 September 2024

et al., 2018). Landslides in these countries are mostly rainfall-triggered, wet landslides, which are sometimes difficult to identify via satellite image or field visits due to factors like heavy rainfall, high cloud cover, revegetation, and shallow seated landslides (Rabby and Li, 2019; Monsieurs et al., 2018). Moreover, these countries often lack the resources to create landslide inventories through field surveys. For these data-sparse, rainfall-induced shallow landslide-prone regions, an alternative method for creating landslide inventories is necessary. An automated landslide detection system that leverages currently available resources could be a viable solution for creating landslide inventories in these regions, helping them mitigate the impact of landslide disasters.

Among data-sparse countries prone to rainfall-induced shallow landslides, Bangladesh is one of the most vulnerable. Neither the government nor any private organization maintains a record of the historical landslide inventories in Bangladesh (Ahmed et al., 2014). As a result, creating landslide inventories is particularly challenging, compounded by three main factors: First, manual collection of landslide inventories is extremely costly and time-consuming (CDMP, 2012); second, the extremely hilly terrain becomes inaccessible during heavy monsoon season when landslides are most likely to occur (Abedin et al., 2020); and third, conflicts in the hilly areas of Bangladesh pose life-threatening risks, hindering traditional data collection methods (Ahmed et al., 2014). In light of these unique circumstances, there is an urgent need for an automated landslide inventory method. Remarkably, despite the importance of this issue, no study has been previously conducted in Bangladesh to detect landslide inventories using an automatic method, highlighting a critical gap in environmental science research. Recognizing this gap, this study selects Bangladesh as a case study to develop a reliable automatic method for detecting rainfall-induced shallow landslides. This approach incorporates advanced geotechnical and geospatial techniques to overcome the limitations of traditional approaches and contribute to the CLDMP.

Landslide detection, also known as creating landslide inventories, has become easier due to recent advancements in remote sensing (RS) (Lu et al., 2023). Several techniques exist for detecting landslides using RS, including visual interpretation, change detection-based approaches, knowledge-based methods, machine learning techniques, and deep learning strategies (Novellino et al., 2024). Although visual interpretation is effective, it requires substantial professional expertise and is resource-intensive (Zhang et al., 2019). Amatya et al. (2022) developed a semi-automated method by modifying three change detection techniques, using pre- and post-satellite images from two different sources, to detect landslides in Vietnam, Laos, Myanmar, and Thailand. They utilized Principal Component Analysis (PCA), Normalize Difference Vegetation Index (NDVI), and Independent Component Analysis (ICA) to detect the change and in turn, landslides. However, change detection-based methods require both pre-event and post-event satellite images, which can be challenging to acquire promptly, especially under poor weather conditions. Obtaining the necessary images immediately after rainfall-induced landslides can be particularly difficult (Lu et al., 2023). Yi et al. (2023) used the interferometric synthetic aperture radar (InSAR) method to develop a semi-automatic landslide detection technique for a part of the Qinghai–Tibet Plateau. While synthetic aperture radar (SAR) data is unaffected by weather conditions, its applicability for detecting landslides is limited due to typically lower accuracies (Deng et al., 2023). Many previous studies have utilized knowledge-based methods, for instance, threshold segmentation, object-based segmentation, and image enhancement (Tehrani et al., 2022). However, these methods are often restricted to specific locations due to limited transferability. In recent decades, machine learning (ML) has emerged as a powerful automated classification approach. Several ML methods are widely used for different purposes, including support vector machines (SVM), random forest (RF), logistic regression (LR), Bayesian classifiers, and so on. For instance, Meena et al. (2022) applied four machine-learning models RF, SVM, Convolutional U-net (CUN), and K-Nearest Neighbor (KNN) to develop an automated landslide detection method using satellite images from two different satellites. They have found CUN to be the best model to detect landslides in Nepal. However, the performance of ML methods depends on the quality of input features and requires rigorous data preprocessing and feature engineering (Ma et al., 2021).

Deep learning (DL) is a cutting-edge technique that can provide reliable solutions for environmental issues by utilizing RS. The integration of DL methods with both object-based and pixel-based approaches addresses challenges associated with conventional approaches, like manual feature extraction and limited adaptability to dynamic environmental conditions (Chen et al., 2018). DL combined with RS allows for data-driven and automated solutions that are adaptable to varied landscapes and temporal scales. Landslide detection can be significantly improved in terms of accuracy and reliability by using DL approaches together with satellite imagery, offering a more comprehensive perspective (Lu et al., 2020).

Several object-based DL methods are used in landslide detection, for instance, Region-based Convolutional Neural Networks (R-CNN) and You Only Look Once (YOLO). However, these methods typically use rectangular bounding boxes in satellite imagery to label the position of landslides (Lu et al., 2023). As a result, these object-based methods cannot detect the exact boundaries of landslides due to the use of rectangular bounding boxes. This is considered a limitation because identifying the precise delineation of landslide boundaries is crucial for a comprehensive understanding of the landslide-affected areas and their associated impacts (Keyport et al., 2018).

Conversely, pixel-based deep learning (DL) methods for landslide detection outperform object-based DL methods due to their fine-grain spatial resolution and applicability in varied landscape conditions (Wen et al., 2021). For instance, the popular pixel-based DL technique, convolutional neural networks (CNN), shows superior performance in automatically capturing detailed terrain variations, which is crucial for identifying the early signs of landslides and accurately delineating their extents (Lu et al., 2023). Feature engineering, which traditionally requires manual intervention, is labor-intensive and demands expert knowledge, but CNNs can now automatically extract relevant features associated with landslides. This advancement contributes significantly to remote sensing (RS) and geospatial analysis in assessing and mitigating natural hazards (Su, 2021). Pixel-based methods thus play a critical role in developing accurate and robust landslide detection approaches by leveraging their ability to extract detailed values, textures, and other spectral characteristics of each pixel, which is essential for identifying patterns in landslide-prone areas (Meena et al., 2023; Ghorbanzadeh et al., 2022). For these reasons, pixel-based DL methods have recently emerged as the most preferred, reliable, and accurate approach for detecting landslides, especially in diverse topographic regions and varied environmental conditions (Meena et al., 2023).

Therefore, the specific objectives of this work are: i) to detect rainfall-induced shallow landslides using a deep learning-based model and by leveraging both multi-temporal, very high-resolution (VHR) PlanetScope and medium-resolution (MR) Sentinel-2 imagery, and ii) to identify the best-performing satellite dataset for landslide detection in the study area. This automated approach would ensure efficient and rapid analysis of extensive datasets, facilitating the timely identification of rainfall-triggered shallow landslides in the study area, with potential applications in a similar geographic context.

2. Materials and methods

2.1. Study area description

The Chittagong Hill Districts (CHD) is the only extensive hilly region in Bangladesh prone to landslides. Located in the southeastern part of the country, it is known for its unique geographical and cultural features. This CHD is divided into two parts based on the types of inhabitants: i) the urbanized hill districts (comprising Chittagong, and Cox's Bazar

districts) and the Chittagong Hill Tracts (CHT), which includes Bandarban, Khagrachari, and Rangamati districts (Fig. 1.) (Ahmed, 2021). The urbanized hill districts are mostly inhabited by Bengalis, and Rohingya refugees (who fled from Myanmar due to ongoing genocide and violence), while the indigenous people primarily reside in the CHT (Ahmed, 2021). This area is surrounded by the Bay of Bengal from its south and southwestern part; Myanmar by its southeastern part; and India by its north and northeast (Fig. 2.). The total area of CHD is 19,888 sq. km with a population of 13,835,544, including both Bengalis and Indigenous people (BBS, 2023). According to a recent report by the Bangladesh Bureau of Statistics (BBS, 2023), the average population density in this region is 979 per sq. km.

Like the rest of Bangladesh, the CHD experiences a tropical monsoon climate with three distinct seasons: the dry season (November to March), the pre-monsoon season (April to May), and the monsoon season (June to October). The average annual monsoon (June–October) rainfall in this region ranges from approximately 2540 to 3810 mm. The area is dominated by undulating hills, with elevations ranging from 80 to 160 m in the Semutang anticline to 650–800 m in the Bandarban anticline (Banglapedia, 2021). These hills are divided into two distinct ranges: the low hills (Dupi Tila and Dihing formation, with elevations below 300m), and the high hills (Surma and Tipam formation, with elevations below 300m) ranges. The region is composed of unconsolidated or semi-consolidated tertiary sedimentary rocks including sandstone, shale, siltstone, and limestones along with pebbles and cobbles (Alam et al., 2003; Brammer, 1986). The presence of these rock types creates a geological environment where slopes are highly sensitive to increased pore water pressure, leading to slope instability. Rainfall serves as a primary trigger for landslides by saturating these materials, reducing shear strength, and ultimately causing slope failure. Dense forests and river valleys are also common features of this extremely hilly region.

It is important to note that various social and environmental issues persist in the CHD, including land disputes, displacement, and environmental degradation. These issues should be the subjects of research and development to improve the well-being of local communities (Ahmed, 2021). The combination of weak lithology, steep slopes, deep valleys,

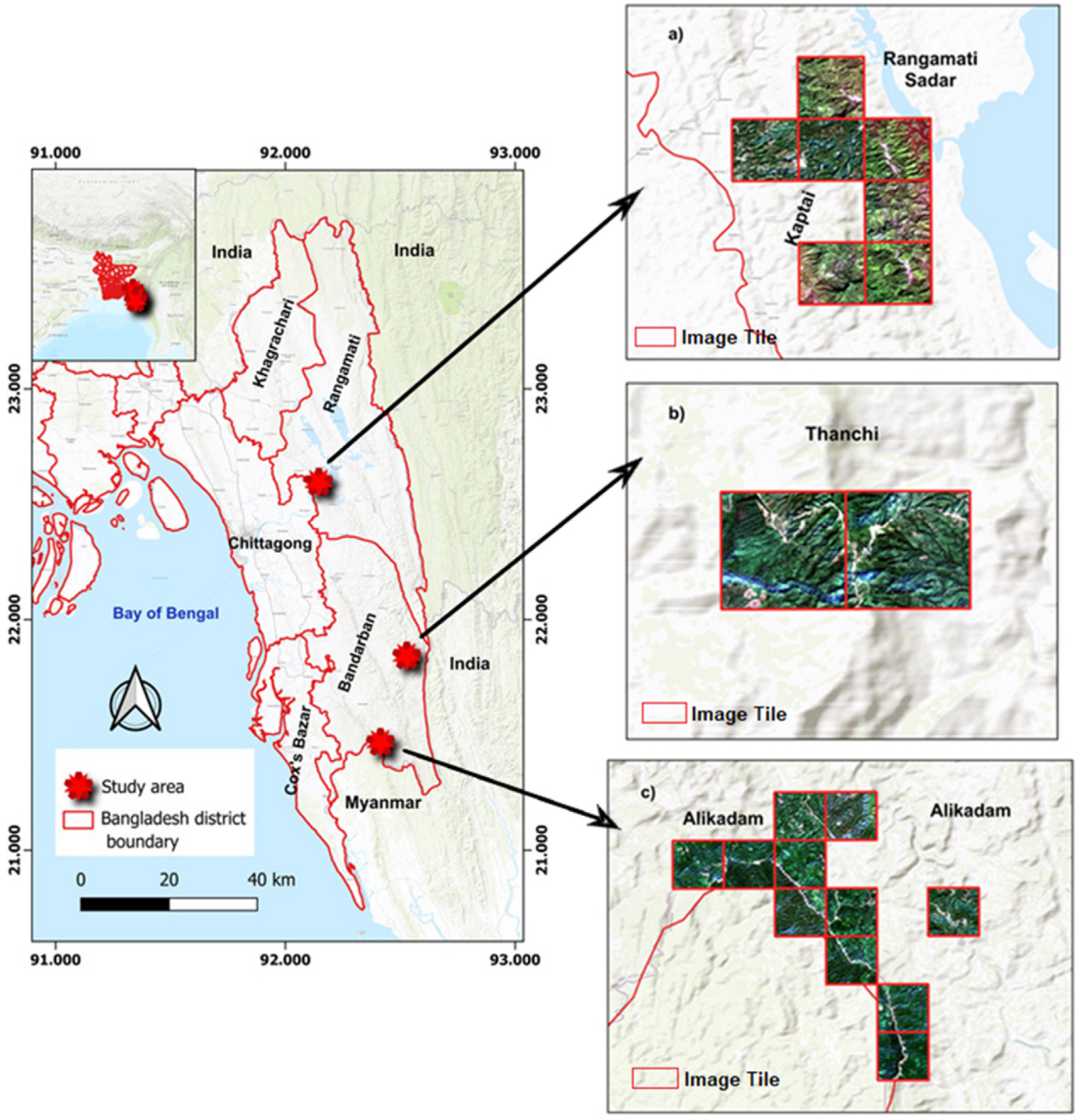

Fig. 1. Map showing the geographical location of the study area.

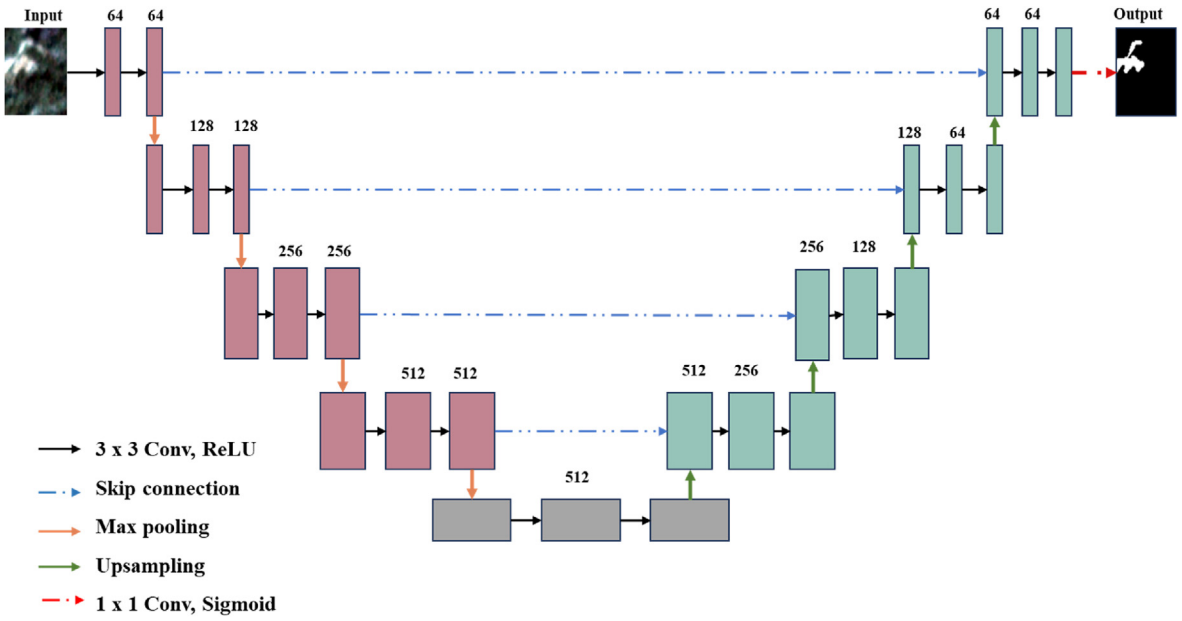

Fig. 2. The U-net structure was utilized in the present study.

and intense monsoon rainfall contributes to the instability of slopes, increasing the risk of frequent and severe landslides, mainly debris flows and rockslides. In recent decades, rapid deforestation and unplanned urbanization have further heightened the region's vulnerability to landslides (Ahmed, 2021). For instance, on June 13, 2017, intense rainfall triggered landslides that resulted in at least 168 fatalities in Rangamati, Chittagong, and Bandarban districts (Ahmed et al., 2018). More recently, in August 2023, landslides and floods claimed the lives of about 51 people in the Bandarban, Rangamati, Cox's Bazar, and Chittagong districts (ReliefWeb, 2023). Therefore, as part of this study, four upazilas from Rangamati (Rangamati Sadar and Kaptai) and Bandarban (Alikadam and Thanchi) districts in the CHT have been selected as case studies.

2.2. U-net model

In recent years, several researchers have worked on developing automatic methods to detect landslides (Table S1). These studies have been conducted in different regions, including China, India, Myanmar, Indonesia, Haiti, Brazil, New Zealand, Japan, Nepal, Papua New Guinea, Congo, and Hong Kong. These areas are dominated by tropical or subtropical monsoon climates; steep slopes; and terrain characterized by sedimentary, metamorphic, and volcanic rocks; and they are particularly affected by debris flow, rock falls, rock slides, mudflows, rock avalanches (Meena et al., 2022, 2023; Lu et al., 2023; Chandra et al., 2023; Xia et al., 2022; Bragagnolo et al., 2021; Wang et al., 2021; Chen et al., 2018a). While simpler models (e.g., logistic regression, SVM, RF) may be suitable for broader classification tasks, they lack the spatial precision needed for accurate pixel-based segmentation, which is critical for detecting small, shallow landslides in areas like Bangladesh (Zhang and Wang, 2024). The U-net model, with its encoder-decoder architecture, excels in capturing spatial hierarchies and complex patterns within high-resolution imagery, significantly improving detection accuracy (Arulananth et al., 2024). Thus, although various DL models have been tested for automatic landslide detection, the U-net model has outperformed others in areas characterized by tropical or subtropical monsoon climates; sedimentary rocks; and rainfall-induced landslides, including both slides and debris flow (these characteristics are similar to the present study area) (Table S1). As a result, the present study employed a U-net model for landslide detection.

U-net, a type of fully CNN, has emerged as one of the most reliable methods for image segmentation in environmental applications. Originally designed for biomedical image segmentation (Ronneberger et al., 2015), U-net has been successfully adapted for landslide detection due to its ability to precisely delineate landslide boundaries at the pixel level (Meena et al., 2022; Nava et al., 2022). Unlike object-based DL methods such as R-CNN and YOLO, which rely on rectangular bounding boxes for classification (Lu et al., 2023), U-net provides detailed pixel-wise classification, which is essential for detecting shallow landslides in high-resolution imagery. This study utilized the U-net model by adopting Python code available on GitHub (Meena et al., 2023), with slight modifications made for this research.

The architectural configuration of the model used in this study incorporates a dual pathway system designed for feature extraction (Fig. 2.). The encoder specializes in capturing low-level representations. Within the encoder path, individual convolution blocks are systematically arranged, each consisting of two convolutional layers with a 3×3 kernel size, followed by a 2×2 max-pooling layer. The activation of these convolutional layers is achieved using the rectified linear unit (ReLU) function. To introduce non-linear downsampling, a 2×2 max-pooling layer is appended after each convolutional block in the encoder path.

In contrast, the decoding path incorporates a 2×2 upsampling layer after each 3×3 convolutional layer, strategically placed to reconstruct high-level representations. In the final layer, a sigmoid function is used to produce class predictions within a probability range of 0–1. Since the primary objective of this study is to detect landslides and non-landslide areas (binary classification), the sigmoid function is applied, as it is suitable for binary classification problems.

The model was meticulously trained using various combinations of hyperparameters to determine the optimal settings. These include batch sizes of 4, 8, 16, and 32; learning rates of 0.01, 0.001, 0.0001, 0.005, and 0.0005; and varying numbers of filters in the first convolutional layer with 4, 8, 16, and 32.

2.3. Loss function

An appropriate loss function is a crucial component of image segmentation to train DL models both accurately and efficiently, enabling them to learn objects from images. Scholars have employed various loss functions tailored to specific tasks. However, the region-based loss functions are more suitable and widely used in RS, more specifically for landslide detection (Meena et al., 2023; Li et al., 2022; Qin et al., 2021;

Prakash et al., 2020).

In this study, a region-based loss function was used to train the U-net model. There are five common region-based loss functions which are Dice loss, Tversky loss, Focal Tversky loss, Sensitivity-Specificity loss, and Log-Cosh Dice loss (Jadon, 2020). However, not all these functions are appropriate for every problem. The input data used in this study is imbalanced, and in such cases, the Dice loss function performs better at handling imbalanced datasets (Li et al., 2019). This function is used for binary classification alongside the U-net model (Xu et al., 2023). Therefore, Dice loss was used in the present work for training the U-net model.

The Dice loss is derived from the dice coefficient, a statistical metric assessing the likeness between two sets of data (Xu et al., 2023). In the context of image segmentation, this coefficient quantifies the similarity between a predicted mask and its corresponding ground truth mask. Mathematically, the dice coefficient is defined in the following Eq. (1):

$$DSC(A,B) = \frac{2(A \cap B)}{A \cup B} \tag{1}$$

Where, *DSC* denotes the dice coefficient of two different datasets, *A* is the predicted dataset, *B* represents the ground truth data, ∩ is the symbol of intersection, and ∪ is the symbol of union. “Intersection” means the number of overlapping pixels between the predicted and ground truth masks, and "Union" denotes the total number of pixels counting from both predicted and ground truth masks. The dice coefficient ranges from 0 to 1, with 1 indicating a perfect match.

The Dice loss is derived from the dice coefficient which is defined by the following Eq. (2):

$$Dice\ Loss = 1 - Dice\ Coefficient \tag{2}$$

The main objective of using the dice loss during the training of the U-net model is to minimize the overall loss so that the small-scale landslides can be detected more accurately.

2.4. Performance evaluation metrics

Accuracy alone cannot be used for a comprehensive performance evaluation of any model, therefore other metrics like precision, recall, and F1 score are used to deal with imbalanced datasets as well as when there is a need to minimize the false positives or false negatives pixels. Therefore, in this study, those metrics have been used to evaluate the overall performance of the model to detect landslides following the Eq. used by Xu et al. (2024). The values of all the metrics mentioned above range from 0 to 1 and are defined as:

$$Precision = \frac{TP}{TP + FP} \tag{3}$$

$$Recall = \frac{TP}{TP + FN} \tag{4}$$

$$F1\ Score = \frac{2 \times Precision \times Recall}{Precision + Recall} \tag{5}$$

$$Accuracy = \frac{TP + TN}{TP + TN + FP + FN} \tag{6}$$

Where, *TP* means true positives (indicates the pixels identified as landslides pixels which are landslides pixels), *TN* means true negative (indicates the pixels identified as non-landslides pixels which are non-landslides pixels), *FN* denotes the false negatives (indicates the pixels identified as non-landslides pixels which are landslides pixels), and *FP* refers to false positives (indicates the pixels identified as landslides pixels which are non-landslides pixels).

For all the four above-mentioned metrics, the closer value to 1 the better, meaning that the model performs well detecting the landslides pixels. Conversely, values closer to 0 indicate the poor performance of the model to detect landslide pixels.

2.5. Data augmentation

It is essential to use as much data as possible to obtain accurate results from any DL model implementation. As this study employed a relatively small dataset, the horizontal flip technique was used to augment the training dataset. Consequently, the number of training samples doubled in each experiment (for instance, if 380 original patches are fed to the model during training, the input increases to 760 with augmentation).

Regarding horizontal flips, each image in the dataset is horizontally mirrored, creating a new version with the left and right reversed. This is achieved by flipping the pixels along a vertical axis. By exposing the model to both the original and horizontally flipped images during training, it becomes more robust and capable of recognizing patterns and features from different perspectives.

2.6. Satellite data

A total of 20 Cloud-free image tiles were collected from the dedicated websites of three satellites: PlanetScope (https://www.planet.com/), Sentinel-2 (https://dataspace.copernicus.eu/), and Advanced Land Observing Satellite Phased Array L-band Synthetic Aperture Radar (ALOS-PALSAR) (https://search.asf.alaska.edu/).

The PlanetScope imagery provides VHR images with a 3m spatial resolution. All image tiles have uniform dimensions of 667 x 667 pixels and have undergone both orthorectification and radiometric correction, as provided by the data providers. The dataset used in this study consists of harmonized images, ensuring a standardized foundation for subsequent analyses.

For this study, Sentinel-2 imagery with a 10m spatial resolution was used. The image tiles are uniformly 200 x 200 pixels in size and have undergone both orthorectification and radiometric correction, except for five image tiles collected on November 15, 2018, from Kaptai and Rangamati Sadar upazilas (Table 1). These tiles lacked atmospheric correction, which was subsequently performed using the Sen2Cor plugin, accessible within the SNAP software provided by the European Space Agency (ESA). Since the spectral bands were downloaded separately, band composition techniques were applied to merge the 4 bands into a single image for each tile through the open-source software QGIS 3.34.1.

The study area is characterized by various types of vegetation, often creating shaded areas. Although red, green, and blue (RGB) bands are generally sufficient for landslide detection, it is challenging to distinguish landslides from the vegetation in shaded areas (Meena et al., 2021). To address this limitation, the near-infrared (NIR) band was used with RGB bands, as the NIR band provides more detailed information like the moisture content of the surface. The combined use of these four bands (RGB and NIR) enhances the accuracy in identifying landslides that might otherwise appear similar to vegetation due to shading.

In this study, a 12.5m resolution DEM derived from ALOS-PALSAR was used, sourced from the Alaska Satellite Facility (ASF) website. Since the study incorporates images with spatial resolutions of 3m

Table 1
Spatiotemporal information of the satellite imagery used in this study.

Number of image tiles	Acquisition date (VHR PlanetScope Imagery)	Acquisition date (MR Sentinel 2 Imagery)	Upazila
8	October 27, 2023	October 20, 2023	Alikadam
3	December 23, 2022	December 24, 2022	Alikadam
1	November 16, 2018	November 15, 2018	Kaptai
4	November 16, 2018	November 15, 2018	Rangamati Sadar
2	January 24, 2019	January 11, 2019	Rangamati Sadar
2	January 8, 2022	January 8, 2022	Thanchi

(PlanetScope) and 10m (Sentinel-2), the DEM was resampled to match these resolutions using QGIS 3.34.1. Elevation and slope were extracted from the DEM and included in the analysis.

2.7. Creation of the ground truth data (landslide masks)

To accurately detect landslides from satellite imagery, the model requires landslide masks during its training and validation phases. Among the 4 major types of landslides (falls, topples, slides, and flows), slides and debris flows dominate in CHD (Rabby & Li, 2019, 2019a). Therefore, this study focused primarily on debris flows, with a smaller number of slide-type landslides for the creation of the landslide masks (Fig. S1).

Landslide masks were created manually for this study. Latitude and longitude data from previous landslide events were collected during field visits by a team of UCL Humanitarian Institute, Department of Risk and Disaster Reduction (RDR) at the University College London (UCL), UK. These points were cross-referenced by leveraging Google Earth Pro to verify landslide occurrences during the corresponding periods.

After verifying the points, polygons were created for the areas where landslides were visible. In each case, polygons were drawn to represent the area affected by the landslide, as observed in Google Earth Pro (Fig. S1.).

The majority of the landslide polygons (151 polygons covering a total area of 225,882 m^2) were created for Alikadam upazila, where landslides occurred in 2023. All but 4 polygons (rock slides in Rangamati Sadar upazila; Fig. S1b.) represent the debris flows (Fig. S1a.). After creating the polygons, they were assigned to the respective image tiles based on location. The polygons were then rasterized employing QGIS 3.34.1, with landslide areas assigned a value of 1, and non-landslide areas assigned a value of 0. The rasterization process was carried out for each image tile at both 3m and 10m spatial resolutions.

Table 2 demonstrates the number of polygons created as landslide masks, along with the time, place, types, and total area (m^2). In total, 181 landslide polygons (total area of 314,523 m^2) were created.

2.8. Repeated stratified hold-out validation

The entire dataset was divided into training (50% of the dataset), validation (25% of the dataset), and testing (25% of the dataset) parts (Fig. 3.). It is called a hold-out validation, as the entire dataset is split into 3 parts and each part used for a specific purpose. The training set is used for training the U-net model to learn the objects from the images. The validation set is used for tuning the hyperparameters of the model with different learning rates, batch sizes, and filters. Finally, the test dataset is used for evaluating the performance of the model.

Given the relatively small dataset, a specific hold-out might produce biased results. To overcome this issue, a stratified hold-out approach was adopted, ensuring that the dataset is approximately balanced across the training, validation, and test sets in terms of the number of landslide samples (Table 3).

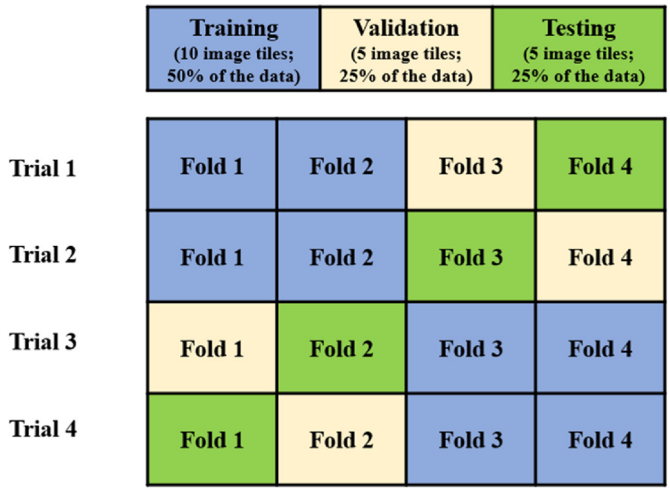

Fig. 3. A repeated stratified hold-out validation method was used in this study.

Fig. 3 represents how the entire dataset was used for experiments. The dataset was partitioned into 4 folds, with each fold containing five image tiles. Each fold was used as a test set at least once during the trials (Table 3). For instance, fold 1 contains the largest number (114 out of 181) of landslide polygons (Table 3). However, folds 3 and 4 contain only 12 landslide polygons each, indicating an imbalanced dataset. Four trials were conducted, with the test dataset rotated in each trial, ensuring that the entire dataset was utilized (Fig. 3.).

In Trial 1, folds 1 and 2 were used for training, fold 3 for validation, and fold 4 for testing. The same approach was applied in subsequent trials, making this process a repeated stratified hold-out validation.

2.9. Experimental setup

This study used four distinct datasets to evaluate their performance, as illustrated in Fig. 4. Dataset A included only the RGB and NIR bands from VHR PlanetScope Imagery. Dataset B included RGB and NIR bands from VHR PlanetScope, along with Elevation, Slope, and the NDVI (calculated from the NIR and red bands). Dataset C included RGB and NIR bands from MR Sentinel-2 Imagery. Dataset D combined Sentinel-2 RGB and NIR bands with Elevation, Slope, and NDVI. In each experiment, the repeated stratified hold-out method was applied to each dataset, resulting in 16 separate experiments (four trials with each dataset).

For Datasets A and B, 100 patches (64 × 64 pixels) were generated from each image tile. During training, 1000 patches were created from 10 image tiles, with 500 patches for validation and 500 for testing (Tables 3

Table 2
Information related to the landslide polygons (masks) used in this study.

Number of image tiles (N = 20)	Number of polygons created as landslide masks (N = 181)	Total landslide area (m^2) (Total area 314,523 m^2)	Year	Type of landslides	Upazila
8	151	225,882	2023	Debris flow	Alikadam
3	11	11,538	2022	Debris flow	Alikadam
1	3	8136	2018	Debris flow	Kaptai
4	5	5256	2018	Debris flow and rock slides	Rangamati Sadar
2	4	49,527	2019	Rock slides	Rangamati Sadar
2	7	14,184	2022	Debris flow	Thanchi

Table 3
Formation of the folds used for the repeated stratified hold-out validation.

Fold number	Number of image tiles	Upazila (from where the image tile was collected)	Year	Number of polygons (landslide masks)
Fold 1	5	Alikadam	2023	114
Fold 2	5	Alikadam	2023 and 2022	43
Fold 3	5	Alikadam, Kaptai, and Rangamati Sadar	2022 and 2018	12
Fold 4	5	Rangamati Sadar, and Thanchi	2018, 2019 and 2022	12

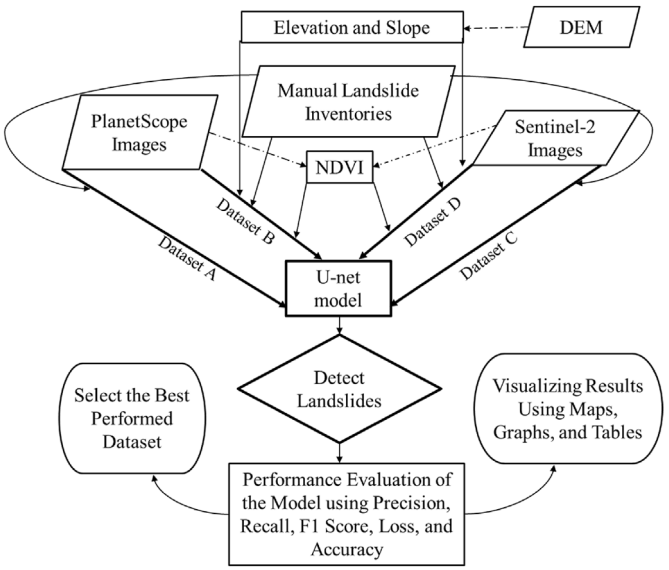

Fig. 4. The flow chart shows the full process of the proposed landslide detection approach.

and 4). For Datasets C and D, 36 patches (32 × 32 pixels) were generated from each image tile, resulting in 360 patches for training, 180 for validation, and 180 for testing (Tables 3 and 4).

Table 4 highlights the differences in the total number of pixels extracted from landslide masks for Datasets A and B compared to Datasets C and D.

3. Results

A total of 16 experiments were conducted utilizing the U-net model, each with different sets of hyperparameter configurations. The configuration was characterized by a filter size of 8, a batch size of 4, a learning rate of 0.01, and the Adam optimizer emerged as, comparatively, the best model across all experiments.

The F1 scores across successive epochs (5 epochs), illustrating the U-net model's performance with the aforementioned hyperparameter set during both training and validation phases for all 16 experiments, are presented in Fig. S2 and S3. In Fig. S2, it can be observed that the F1 score shows an upward trend in Trials 1 and 2 for both Datasets A and B. However, in Trials 3 and 4, the F1 score does not improve sufficiently, indicating that landslide detection in these trials may be unreliable Trials (3 and 4). Nevertheless, in Fig. S3., the F1 score shows an upward curve in all trials in both Datasets C and D. Fig. S4 displays the loss curve throughout epochs, outlining the optimization evolution of the model under the same set of hyperparameters across all experimental trials for the Datasets A and B. The loss curves in Trials 1 and 2 show a downward trend, indicating successful landslide detection with Datasets A and B. Furthermore, in Trials 1 and 2 with Dataset C, and Trials 1, 2, and 3 with Dataset D, the model produced proper downward loss curves (Fig. S5.).

The evaluation metrics for landslide detection in the 16 experiments are presented in Table 5. Table 5 demonstrates precision, recall, F1 score, loss, and accuracy metrics during the testing phase. Fig. 5 and 6. visually represent the areas identified as landslides across the 16 experiments, utilizing the U-net model. Notably, Datasets A and B, comprising VHR imagery from PlanetScope, yielded consistent findings across all 4 trials.

Table 5
Precision, Recall, F1 score, Loss, and Accuracy of 16 experimental test datasets.

Trial number	Precision	Recall	F1 score	Loss	Accuracy
Dataset A					
1	***1***	***0.625***	***0.625***	***0.381***	***0.999***
2	***1***	***0.625***	***0.625***	***0.383***	***0.997***
3	1	0.062	0.062	0.958	0.993
4	1	0.375	0.375	0.634	0.996
Mean	1	0.422	0.422	0.589	0.996
Std	0	0.231	0.231	0.237	0.002
Dataset B					
1	***1***	***0.625***	***0.625***	***0.380***	***0.999***
2	***1***	***0.625***	***0.625***	***0.383***	***0.997***
3	1	0.062	0.062	0.958	0.993
4	1	0.375	0.375	0.634	0.996
Mean	1	0.422	0.422	0.589	0.996
Std	0	0.231	0.231	0.237	0.002
Dataset C					
1	1	0.167	0.167	0.998	0.999
2	***1***	***0.333***	***0.333***	***0.700***	***0.997***
3	0.004	0.955	0.009	0.996	0.055
4	0.056	0.111	0.059	0.992	0.976
Mean	0.515	0.392	0.142	0.922	0.757
Std	0.485	0.335	0.124	0.128	0.405
Dataset D					
1	1	0.167	0.167	0.785	0.999
2	***1***	***0.333***	***0.333***	***0.717***	***0.997***
3	0.004	0.955	0.009	0.996	0.055
4	0.711	0.004	0.008	0.991	0.995
Mean	0.679	0.365	0.129	0.872	0.762
Std	0.407	0.360	0.134	0.124	0.408

For Datasets A and B, the mean precision, recall, F1 score, loss, and accuracy metrics across Trials 1, 2, 3, and 4 are 1, 0.422, 0.422, 0.589, and 0.996, respectively (Table 5). Precision is consistently high, near 1, indicating the model tends not to produce false positive landslide pixels. The standard deviation (std) for precision, recall, F1 score, loss, and accuracy in Datasets A and B across Trials 1, 2, 3, and 4 are 0, 0.231, 0.231, 0.237, and 0.002, respectively. Remarkably, Trials 1 and 2 show better performance in landslide detection compared to Trials 3 and 4.

It is important to note that the landslide pixels used in Trials 3 and 4 for training the U-net model were significantly fewer than in Trials 1 and 2 (Table 4). Trials 1 and 2, with more training samples than testing samples, performed better; whereas Trials 3 and 4, with the opposite configuration, exhibited poorer performance in detecting landslides on Datasets A and B (Fig. 5.).

Considering the impact of training sample size on the U-net model's performance, Trials 1 and 2 from Datasets A and B are deemed acceptable for landslide detection in the current study area. Consequently, the mean precision, recall, F1 score, loss, and accuracy metrics for both Datasets A and B, based on Trials 1 and 2, are 1, 0.625, 0.625, 0.380, and 0.999, respectively. The std values for precision, recall, F1 score, loss, and accuracy in Datasets A and B based on Trials 1 and 2 are 0, 0, 0, 0.001, and

Table 4
Total number of pixels used as landslide samples.

Trial Number	Datasets A and B			Datasets C and D		
	Training (1000 patches)	Validation (500 patches)	Testing (500 patches)	Training (360 patches)	Validation (180 patches)	Testing (180 patches)
1	25,935	7161	1851	2309	635	161
2	25,935	1851	7161	2309	161	635
3	9012	10,467	15,468	796	939	1370
4	9012	15,468	10,467	796	1370	939

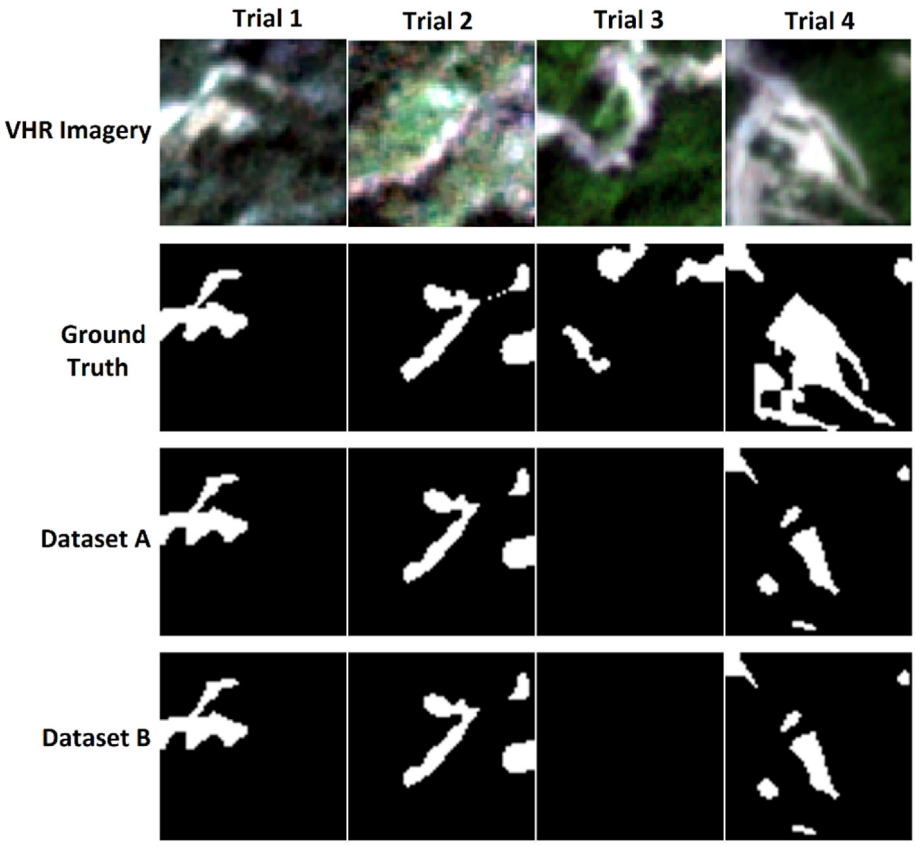

Fig. 5. Landslide detection results getting from using Datasets A, and B in 4 trials.

0.001, respectively, highlighting the reliability of these results. Fig. 5 visually supports the close alignment between the model's landslide detection and the ground truth. Fig. S6 compares the landslide detection by the U-net model, experimented with Dataset A in Trials 1 and 2, with the ground truth over a whole image tile.

Datasets C and D yielded comparatively poorer results than Datasets A and B, as illustrated in Fig. 6 and Table 5. It is crucial to highlight that Datasets C and D consist of MR Imagery obtained from Sentinel-2. Similar to Datasets A and B, the model produced largely analogous outcomes for Datasets C and D, except in Trial 4 (Table 5). The mean precision, recall, F1 score, loss, and accuracy metrics across Trials 1, 2, 3, and 4 for Dataset C, are 0.515, 0.392, 0.142, 0.922, and 0.757, respectively (Table 5). The std values for these metrics across the same trials are 0.485, 0.335, 0.124, 0.128, and 0.405, respectively (Table 5). In Trials 1 and 3, the model did not detect any landslide areas utilizing both Datasets C and D (Fig. 6.). Conversely, in Trial 2, the U-net model identified a few landslide pixels in both datasets. However, in Trial 4, the model incorrectly classified some non-landslide areas as landslides, rendering the results unacceptable (Fig. 6).

4. Discussion

This is evident that DL models perform better with larger training datasets (Ahmed et al., 2023). Meena et al. (2022) revealed similar findings, showing that the size of training samples significantly influences the performance of the DL model in detecting landslides, with larger sets yielding better results. This study also found similar findings that the model performed reliably with Datasets A and B in Trials 1 and 2. Hence, it can be concluded that DL models like U-net should be trained with more samples to achieve reliable accuracy.

The values of evaluation metrics are crucial for judging the performance of a model. In geospatial research, achieving a perfect score of 100 or even close to 100 percent is typically unattainable. RS data, commonly used in geospatial studies, are collected from space via satellites, and are not 100 percent accurate, except for some very high-resolution imagery, such as Pleiades. Consequently, when these RS data layers are utilized in studies, the model's performance tends to decrease by a certain percentage. Therefore, evaluation metrics like the F1 score, recall, and precision mostly range between 50 and 80 percent, as observed in this study. Meena et al. (2023) used 5 U-net-based models to detect both rainfall and earthquake-induced landslides across different regions, utilizing RGB and NIR bands from PlanetScope imagery and a larger set of landslides samples. The five models U-net, Attention U-Net, Attention Res U-Net, and Attention Deep Supervision Multi-Scale (ADSMS) models produced F1 scores of 0.7904, 0.6825, 0.7446, 0.6477, and 0.6576, respectively. These F1 scores are comparable to the 0.625 F1 score achieved in this study using Datasets A and B. However, Yang et al. (2022), using U-Net, DeepLabv3+, PSPNet to automatically detect landslides in China found that the PSPNet performed better.

Bhuyan et al. (2023), using only the optical (RGB) bands of PlanetScope imagery in Japan, Nepal, New Zealand, and Papua New Guinea, found that the U-net-based ADSMS model performed well (F1 score 0.8) for detecting earthquake-triggered landslides. Additionally, Meena et al. (2022) conducted a study in Rasuwa, Nepal, using VHR RapidEye imagery (5m of spatial resolution) and ALOS PALSAR DEM to detect landslides. Two datasets were created: i) RapidEye spectral bands (RGB, NIR, and red-edge), and ii) RapidEye spectral bands plus elevation and slope data from ALOS PALSAR DEM. U-net outperformed ML models in both datasets, with Dataset 1 yielding better results than Dataset 2. The F1 scores produced by Meena et al. (2022) (0.711 without elevation and slope data; and 0.694 with them) are compatible with the F1 score (0.625) produced in the present study. This suggests that the inclusion of elevation and slope data does not necessarily improve landslide detection, as RGB and NIR bands alone are sufficient (Meena et al., 2023).

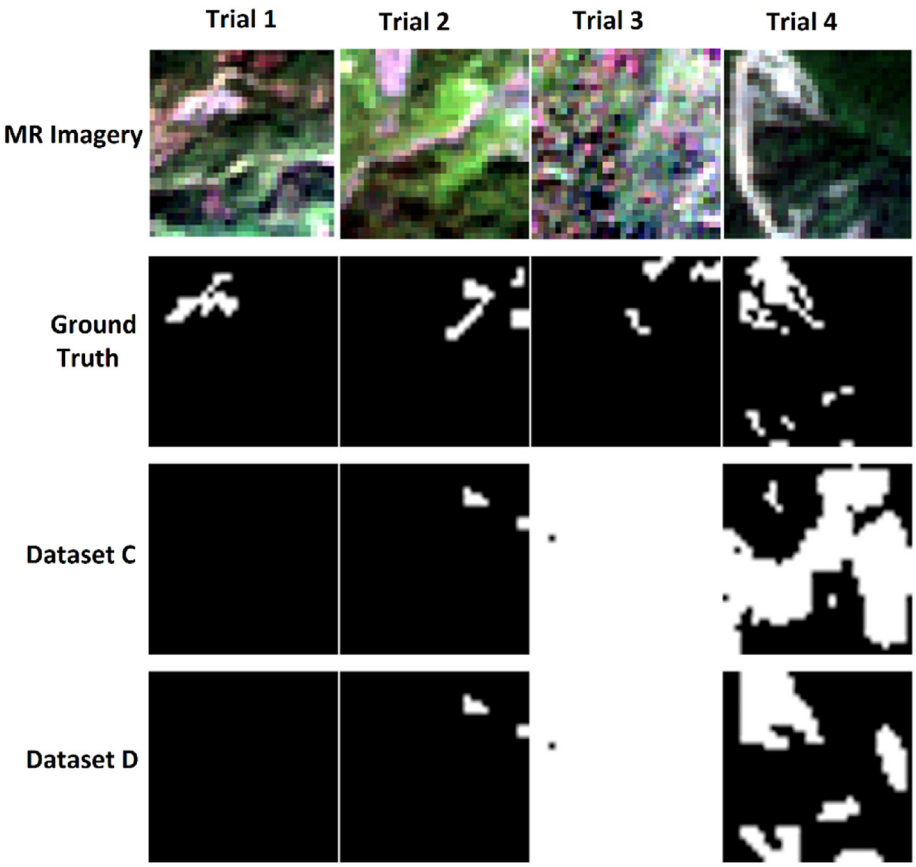

Fig. 6. Landslide detection results getting from using Datasets C, and D in 4 trials.

Another factor that may contribute to the results observed in this study is the size of the image patches. In this analysis, each patch corresponds to dimensions of 64x64 pixels for PlanetScope imagery and 32x32 pixels for Sentinel-2, both of which are relatively small. Larger patch sizes encompass a greater spatial area, allowing for more contextual information to be captured within each patch. In contrast, with smaller patch sizes, variations in elevation—critical for understanding landslide susceptibility—are often minimal or absent. Consequently, the DL model may struggle to establish meaningful relationships between elevation differences and the likelihood of landslide occurrence within a single patch, limiting its predictive performance.

Lu et al. (2023) conducted a study in Wu den, China, and Iburi in Japan to detect landslides automatically by leveraging the MR Sentinel-2 imagery and the National Aeronautics and Space Administration (NASA) provided DEM. They have modified the original U-net model to a dual encoder U-net model. Their model achieved competitive results (precision, recall, and F1 score of 0.783, 0.801, and 0.792, respectively) for detecting earthquake-induced landslides. Xia et al. (2022) also utilized Sentinel-2 imagery for detecting earthquake-induced landslides using several DL models, with DenseNet201 performing best, achieving values of 0.934, 0.8448, 0.8872, and 0.9172 values, respectively, for precision, recall, F1 score, and accuracy.

Previous studies using Sentinel-2 imagery have primarily focused on detecting earthquake-triggered landslides (Lu et al., 2023; Xia et al., 2022; Jelének and Kopačková-Strnadová, 2021). However, detecting rainfall-induced shallow landslides in this study area is challenging due to the small size of affected areas and the limitations of Sentinel-2's spatial resolution (Abedin et al., 2020; Kamal et al., 2022). Sentinel-2's moderate resolution (MR) imagery, with 10m spatial resolution, contains less detailed information and is less suitable for detecting rainfall-induced shallow landslides (Lanaras et al., 2018; Das and Wegmann, 2022).

Furthermore, temporal resolution—the frequency of satellite revisits—plays a critical role in landslide mapping, particularly for shallow, rainfall-induced landslides (Novellino et al., 2024). Additionally, high cloud cover can delay data collection, reducing the accuracy of landslide detection as landslide indicators may disappear due to vegetation regrowth or human activity (Zhang et al., 2020). These issues do not generally affect earthquake-triggered landslide detection. For these reasons, Sentinel-2 did not perform well in this study, indicating less suitable for detecting rainfall-induced shallow landslides.

In contrast, the superior spatial (VHR) and temporal (daily) resolution of PlanetScope imagery facilitate the detection of shallow landslides. Its smaller size pixels provide detailed information and the higher data availability enables the collection of more accurate data (Mueting and Bookhagen, 2023). Although Sentinel-2 includes additional spectral bands, its lower spatial resolution limits precise boundary delineation and accurate localization of landslides (Meena et al., 2023). The key attributes of PlanetScope imagery, such as its competitive spatial resolution, and daily temporal coverage, enhance its effectiveness in detecting landslides by clearly delineating their boundaries. Furthermore, the standardized sensors across PlanetScope satellites simplify and enhance the accuracy of image pre-processing and orthorectification which has eased the overall process of landslide detection (Meena et al., 2023).

Therefore, it can be concluded from the above results and discussion that PlanetScope images are optimal for detecting rainfall-induced shallow landslides. Moreover, for an effective implementation of a DL model like U-net, a higher number of training samples representing landslides is considered crucial to achieving acceptable and reliable results. As well as, it is not essential to the inclusion of elevation, slope, and NDVI to enhance the accuracy, rather the spectral bands RGB and NIR of VHR Imagery are enough to detect landslides. Therefore, landslide detection performance on Datasets A and B was better than on Datasets C and D, as expected (Table 5).

4.1. Limitations of this study

Several limitations in this study impact the accuracy of the experimental findings. The main challenge was manually delineating landslide polygons, which were used as landslide masks (ground truth data). Uncertainties introduced by satellite imagery, primarily due to clouds, led to selecting an image date far from the actual landslide event to ensure cloud-free conditions. The inability to conduct on-site field observations further hindered the verification of precise landslide boundaries when creating the masks, even though the latitude and longitude of the landslides were known. Various factors, such as mapping scale, date, and satellite image quality, affected the precision of landslide detection. The radiometric resolution of the images also influenced the creation of manual inventories.

Additionally, DL requires large datasets, which were not available for this study due to the limited number of landslide masks. Even with the VHR PlanetScope imagery, shallow landslides are sometimes difficult to detect, and finer-resolution imagery, such as Maxar or Pleiades, may be necessary. Besides, this study relied on ALOS PALSAR DEM which has certain limitations according to scholars. All of these factors made it challenging to accurately detect rainfall-induced shallow landslides in this study. Finally, this study used only one DL model to detect landslides.

4.2. Future works

To overcome the limitations of this study, future research should apply more data augmentation techniques to synthetically increase the number of training samples. Additionally, future studies should incorporate both channel and spatial attention layers into the U-net model to focus on important features and discard irrelevant ones, improving model performance and accuracy. Experiments using DEM data provided by the Shuttle Radar Topography Mission (SRTM) should also be explored. Finally, testing other DL models could reveal their effectiveness in detecting landslides in the study area.

5. Conclusion

This study systematically applied the U-net model across 16 experiments to detect rainfall-induced shallow landslides, evaluating its performance using diverse hyperparameters. The optimal configuration was identified with a filter size of 8, a batch size of 4, a learning rate of 0.01, and the Adam optimizer. Training the model with the Dice loss function allowed for precise feature learning, and performance was measured using precision, recall, F1 score, and accuracy metrics.

The results demonstrated that Datasets A and B, which used very high-resolution (VHR) PlanetScope imagery, consistently outperformed other datasets. Specifically, Trials 1 and 2, with larger training samples, yielded the highest accuracy, F1 score, and recall, emphasizing the importance of adequate training data in deep learning models. The mean precision, recall, F1 score, loss, and accuracy for these trials were 1, 0.625, 0.625, 0.380, and 0.999, respectively. Conversely, Datasets C and D, which used lower-resolution Sentinel-2 imagery, produced poorer results, highlighting the critical role of high spatial and temporal resolution in detecting small-scale shallow landslides.

In summary, this study underscores the effectiveness of VHR PlanetScope imagery for automatic detection of rainfall-induced shallow landslides, making the process more reliable and accurate. The findings suggest that the integration of topographic data (e.g., DEM) with PlanetScope imagery does not significantly enhance accuracy; the spectral bands alone are sufficient for this task. Importantly, the results also emphasize that larger training datasets are crucial for improving model performance. Future work should focus on expanding the dataset and exploring additional deep learning techniques to further refine landslide detection in data-sparse regions.

The use of VHR satellite imagery, particularly PlanetScope, combined with deep learning models like U-net, offers a robust solution for detecting rainfall-induced shallow landslides in data-sparse contexts. This approach is suitable for both operational landslide monitoring and research purposes, particularly in areas where traditional data collection methods are not feasible. High-resolution data and large training samples are key to achieving precise and reliable results, while adding topographic information may not always enhance detection accuracy.

Data availability

The code used in the present work is found on the following GitHub repository: https://github.com/RoquiaSalam/A-deep-learning-method-in-automatically-detecting-rainfall-induced-shallow-landslides. A part (PlanetScope) of the whole dataset is also found on the same repository. The whole datasets used in the present work can be obtained on request from the corresponding author.

Funding

Except for the Erasmus Mundus Scholarship, this research did not receive any specific grant from funding agencies in the public, commercial, or not-for-profit sectors.

CRediT authorship contribution statement

Roquia Salam: Writing – original draft, Visualization, Software, Resources, Methodology, Formal analysis, Data curation, Conceptualization. **Filiberto Pla:** Writing – review & editing, Supervision, Project administration, Investigation, Conceptualization. **Bayes Ahmed:** Writing – review & editing, Supervision, Resources, Project administration, Investigation, Conceptualization. **Marco Painho:** Writing – review & editing, Supervision, Investigation.

Declaration of competing interest

The authors declare that there is no conflict of interest among the authors to publish the work.

Acknowledgment

This work is the MSc thesis of Roquia Salam and she is grateful to the European Union (EU), European Commission for fully funding her Master's program (Geospatial Technologies) by awarding the Erasmus Mundus Scholarship.

Appendix A. Supplementary data

Supplementary data to this article can be found online at https://doi.org/10.1016/j.nhres.2024.09.001.

References

Abedin, J., Rabby, Y.W., Hasan, I., Akter, H., 2020. An investigation of the characteristics, causes, and consequences of June 13, 2017, landslides in Rangamati District Bangladesh. Geoenvironmental Disasters 7, 1–19. https://doi.org/10.1186/s40677-020-00161-z.

Ahmed, B., 2021. The root causes of landslide vulnerability in Bangladesh. Landslides 18 (5), 1707–1720. https://doi.org/10.1007/s10346-020-01606-0.

Ahmed, B., Rahman, M.S., Islam, R., Sammonds, P., Zhou, C., Uddin, K., Al-Hussaini, T.M., 2018. Developing a dynamic Web-GIS based landslide early warning system for the Chittagong Metropolitan Area, Bangladesh. ISPRS Int. J. Geo-Inf. 7 (12), 485. https://doi.org/10.3390/ijgi7120485.

Ahmed, B., Rahman, M.S., Rahman, S., Huq, F.F., Ara, S., 2014. Landslide Inventory Report of Chittagong Metropolitan Area. Bangladesh.

Ahmed, S.F., Alam, M.S.B., Hassan, M., Rozbu, M.R., Ishtiak, T., Rafa, N., Mofijur, M., Shawkat Ali, A.B.M., Gandomi, A.H., 2023. Deep learning modelling techniques: current progress, applications, advantages, and challenges. Artif. Intell. Rev. 56 (11), 13521–13617. https://doi.org/10.1007/s10462-023-10466-8.

Alam, M., Alam, M.M., Curray, J.R., Chowdhury, M.L.R., Gani, M.R., 2003. An overview of the sedimentary geology of the Bengal Basin in relation to the regional tectonic

framework and basin-fill history. Sediment. Geol. 155 (3–4), 179–208. https://doi.org/10.1016/S0037-0738(02)00180-X.
Amatya, P., Kirschbaum, D., Stanley, T., 2022. Rainfall-induced landslide inventories for Lower Mekong based on Planet imagery and a semi-automatic mapping method. Geoscience Data Journal 9 (2), 315–327. https://doi.org/10.1002/gdj3.145.
Arulananth, T.S., Kuppusamy, P.G., Ayyasamy, R.K., Alhashmi, S.M., Mahalakshmi, M., Vasanth, K., Chinnasamy, P., 2024. Semantic segmentation of urban environments: leveraging U-Net deep learning model for cityscape image analysis. PLoS One 19 (4), e0300767. https://doi.org/10.1371/journal.pone.0300767.
Banglapedia, 2021. Geological Structure. Encyclopedia of Bangladesh.
BBS, 2023. Population and Housing Census 2022, National Report (Volume I). Bangladesh Bureau of Statistics (BBS), Statistics and Informatics Division (SID), Ministry of Planning. Dhaka, Bangladesh.
Bhuyan, K., Tanyaş, H., Nava, L., Puliero, S., Meena, S.R., Floris, M., Van Westen, C., Catani, F., 2023. Generating multi-temporal landslide inventories through a general deep transfer learning strategy using HR EO data. Sci. Rep. 13 (1), 162. https://doi.org/10.1038/s41598-022-27352-y.
Bragagnolo, L., Rezende, L.R., Da Silva, R.V., Grzybowski, J.M.V., 2021. Convolutional neural networks applied to semantic segmentation of landslide scars. Catena 201, 105189. https://doi.org/10.1016/j.catena.2021.105189.
Brammer, H., 1986. Reconnaissance Soil and Land use survey: Chittagong Hill Tracts (1964–1965). Soil Resources Development Institute, Bangladesh.
Casagli, N., Intrieri, E., Tofani, V., Gigli, G., Raspini, F., 2023. Landslide detection, monitoring and prediction with remote-sensing techniques. Nat. Rev. Earth Environ. 4 (1), 51–64. https://doi.org/10.1038/s43017-022-00373-x.
CDMP, I., 2012. Landslide inventory and Landuse mapping. In: DEM Preparation, Precipitation Threshold Value and Establishment of Early Warning Device. Ministry of Food and Disaster Management, Disaster Management and Relief Division, Government of the People's Republic of Bangladesh, vol. 1, pp. 310–324.
Chandra, N., Sawant, S., Vaidya, H., 2023. An efficient u-net model for improved landslide detection from satellite images. PFG–Journal of Photogrammetry. Remote Sensing and Geoinformation Science 91 (1), 13–28. https://doi.org/10.1007/s41064-023-00232-4.
Chen, G., Weng, Q., Hay, G.J., He, Y., 2018. Geographic object-based image analysis (GEOBIA): emerging trends and future opportunities. GIScience Remote Sens. 55 (2), 159–182. https://doi.org/10.1080/15481603.2018.1426092.
Chen, Z., Zhang, Y., Ouyang, C., Zhang, F., Ma, J., 2018a. Automated landslides detection for mountain cities using multi-temporal remote sensing imagery. Sensors 18 (3), 821. https://doi.org/10.3390/s18030821.
Das, R., Wegmann, K.W., 2022. Evaluation of machine learning-based algorithms for landslide detection across satellite sensors for the 2019 Cyclone Idai event, Chimanimani District, Zimbabwe. Landslides 19 (12), 2965–2981. https://doi.org/10.1007/s10346-022-01912-9.
Deng, J., Dai, K., Liang, R., Chen, L., Wen, N., Zheng, G., Xu, H., 2023. Interferometric synthetic aperture radar applicability analysis for potential landslide identification in steep mountainous areas with C/L band data. Rem. Sens. 15 (18), 4538. https://doi.org/10.3390/rs15184538.
Ghorbanzadeh, O., Shahabi, H., Crivellari, A., Homayouni, S., Blaschke, T., Ghamisi, P., 2022. Landslide detection using deep learning and object-based image analysis. Landslides 19 (4), 929–939. https://doi.org/10.1007/s10346-021-01843-x.
Herrera, G., Mateos, R.M., García-Davalillo, J.C., Grandjean, G., Poyiadji, E., Maftei, R., Filipciuc, T.C., Jemec Auflič, M., Jež, J., Podolszki, L., Trigila, A., 2018. Landslide databases in the geological surveys of europe. Landslides 15, 359–379. https://doi.org/10.1007/s10346-017-0902-z.
Jadon, S., 2020. A survey of loss functions for semantic segmentation. In: 2020 IEEE Conference on Computational Intelligence in Bioinformatics and Computational Biology (CIBCB). IEEE, pp. 1–7. https://doi.org/10.1109/CIBCB48159.2020.9277638.
Jelének, J., Kopačková-Strnadová, V., 2021. Synergic use of Sentinel-1 and Sentinel-2 data for automatic detection of earthquake-triggered landscape changes: a case study of the 2016 Kaikoura earthquake (Mw 7.8), New Zealand. Remote Sensing of Environment 265, 112634. https://doi.org/10.1016/j.rse.2021.112634.
Kamal, A.M., Hossain, F., Rahman, M.Z., Ahmed, B., Sammonds, P., 2022. Geological and soil engineering properties of shallow landslides occurring in the Kutupalong Rohingya Camp in Cox's Bazar, Bangladesh. Landslides 19 (2), 465–478. https://doi.org/10.1007/s10346-021-01810-6.
Karimi, B., Yanchuck, M., Foust, J., 2019. A new landslide inventory and improved susceptibility model for northeastern Pennsylvania. Environ. Geosci. 26 (4), 125–145. https://doi.org/10.1306/eg.09191919008.
Keyport, R.N., Oommen, T., Martha, T.R., Sajinkumar, K.S., Gierke, J.S., 2018. A comparative analysis of pixel-and object-based detection of landslides from very high-resolution images. International journal of applied earth observation and geoinformation 64, 1–11.
Kumar, A., Asthana, A.K.L., Priyanka, R.S., Jayangondaperumal, R., Gupta, A.K., Bhakuni, S.S., 2017. Assessment of landslide hazards induced by extreme rainfall event in Jammu and Kashmir Himalaya, northwest India. Geomorphology 284, 72–87. https://doi.org/10.1016/j.geomorph.2017.01.003.
Lanaras, C., Bioucas-Dias, J., Galliani, S., Baltsavias, E., Schindler, K., 2018. Super-resolution of Sentinel-2 images: learning a globally applicable deep neural network. ISPRS J. Photogrammetry Remote Sens. 146, 305–319. https://doi.org/10.1016/j.isprsjprs.2018.09.018.
Li, H., He, Y., Xu, Q., Deng, J., Li, W., Wei, Y., 2022. Detection and segmentation of loess landslides via satellite images: a two-phase framework. Landslides 19 (3), 673–686. https://doi.org/10.1007/s10346-021-01789-0.
Li, X., Sun, X., Meng, Y., Liang, J., Wu, F., Li, J., 2019. Dice loss for data-imbalanced NLP tasks. arXiv preprint arXiv:1911.02855. https://doi.org/10.48550/arXiv.1911.02855.
Lu, H., Ma, L., Fu, X., Liu, C., Wang, Z., Tang, M., Li, N., 2020. Landslides information extraction using object-oriented image analysis paradigm based on deep learning and transfer learning. Rem. Sens. 12 (5), 752.
Lu, W., Hu, Y., Zhang, Z., Cao, W., 2023. A dual-encoder U-Net for landslide detection using Sentinel-2 and DEM data. Landslides 20 (9), 1975–1987. https://doi.org/10.1007/s10346-023-02089-5.
Ma, Z., Mei, G., Piccialli, F., 2021. Machine learning for landslides prevention: a survey. Neural Comput. Appl. 33 (17), 10881–10907. https://doi.org/10.1007/s00521-020-05529-8.
Meena, S.R., Ghorbanzadeh, O., van Westen, C.J., Nachappa, T.G., Blaschke, T., Singh, R.P., Sarkar, R., 2021. Rapid mapping of landslides in the Western Ghats (India) triggered by 2018 extreme monsoon rainfall using a deep learning approach. Landslides 18, 1937–1950. https://doi.org/10.1007/s10346-020-01602-4.
Meena, S.R., Nava, L., Bhuyan, K., Puliero, S., Soares, L.P., Dias, H.C., Floris, M., Catani, F., 2023. HR-GLDD: a globally distributed dataset using generalized DL for rapid landslide mapping on HR satellite imagery. Earth Syst. Sci. Data Discuss. 2022, 1–21. https://doi.org/10.5194/essd-15-3283-2023.
Meena, S.R., Soares, L.P., Grohmann, C.H., Van Westen, C., Bhuyan, K., Singh, R.P., Floris, M., Catani, F., 2022. Landslide detection in the Himalayas using machine learning algorithms and U-Net. Landslides 19 (5), 1209–1229. https://doi.org/10.1007/s10346-022-01861-3.
Mondini, A.C., Guzzetti, F., Melillo, M., 2023. Deep learning forecast of rainfall-induced shallow landslides. Nat. Commun. 14 (1), 2466. https://doi.org/10.1038/s41467-023-38135-y.
Monsieurs, E., Jacobs, L., Michellier, C., Basimike Tchangaboba, J., Ganza, G.B., Kervyn, F., Maki Mateso, J.C., Mugaruka Bibentyo, T., Kalikone Buzera, C., Nahimana, L., Ndayisenga, A., 2018. Landslide inventory for hazard assessment in a data-poor context: a regional-scale approach in a tropical African environment. Landslides 15, 2195–2209. https://doi.org/10.1007/s10346-018-1008-y.
Mueting, A., Bookhagen, B., 2023. Tracking Slow-Moving Landslides with PlanetScope Data: New Perspectives on the Satellite's Perspective. EGUsphere, pp. 1–36. https://doi.org/10.5194/egusphere-2023-1698, 2023.
Nava, L., Bhuyan, K., Meena, S.R., Monserrat, O., Catani, F., 2022. Rapid mapping of landslides on SAR data by attention U-Net. Rem. Sens. 14 (6), 1449. https://doi.org/10.3390/rs14061449.
Novellino, A., Pennington, C., Leeming, K., Taylor, S., Alvarez, I.G., McAllister, E., Arnhardt, C., Winson, A., 2024. Mapping landslides from space: a review. Landslides 1–12. https://doi.org/10.1007/s10346-024-02215-x.
Prakash, N., Manconi, A., Loew, S., 2020. Mapping landslides on EO data: performance of deep learning models vs. traditional machine learning models. Rem. Sens. 12 (3), 346. https://doi.org/10.3390/rs12030346.
Qin, S., Guo, X., Sun, J., Qiao, S., Zhang, L., Yao, J., Cheng, Q., Zhang, Y., 2021. Landslide detection from open satellite imagery using distant domain transfer learning. Rem. Sens. 13 (17), 3383. https://doi.org/10.3390/rs13173383.
Rabby, Y.W., Li, Y., 2019. An integrated approach to map landslides in Chittagong Hilly Areas, Bangladesh, using Google Earth and field mapping. Landslides 16 (3), 633–645. https://doi.org/10.1007/s10346-018-1107-9.
Rabby, Y.W., Li, Y., 2019a. Landslide inventory (2001–2017) of Chittagong hilly areas, Bangladesh. Data 5 (1), 4. https://doi.org/10.3390/data5010004.
ReliefWeb, 2023. Chattogram division flash floods and monsoon rain - HCTT humanitarian response plan 2023 (August 2023-january 2024), Bangladesh. https://reliefweb.int/report/bangladesh/chattogram-division-flash-floods-and-monsoon-rain-hctt-humanitarian-response-plan-2023-august-2023-january-2024?fbclid=IwZXh0bgNhZW0CMTAAAR0orUDUIG6Weym5LEK6kz66a0HTbnpZsrndSCt6g_fJg0G4BYRTFZNMuqY_aem_AWoYX5l1iemMbVtv7PJ4dxjOv55p1C1sMx1elGtgTqCMf62cWbQSBC-EzL1QPqiVo_G9E9y17kijQuyNHMiSMT-k.
Ronneberger, O., Fischer, P., Brox, T., 2015. U-net: convolutional networks for biomedical image segmentation. In: Medical Image Computing and Computer-Assisted Intervention–MICCAI 2015: 18th International Conference, Munich, Germany, October 5-9, 2015, Proceedings, Part III, vol. 18. Springer International Publishing, pp. 234–241. https://doi.org/10.1007/978-3-319-24574-4_28.
Su, Z., 2021. Advanced 2D and 3D Computer Vision for a Smarter City-From Image to Point Cloud. Hong Kong University of Science and Technology, Hong Kong.
Tehrani, F.S., Calvello, M., Liu, Z., Zhang, L., Lacasse, S., 2022. Machine learning and landslide studies: recent advances and applications. Nat. Hazards 114 (2), 1197–1245. https://doi.org/10.1007/s11069-022-05423-7.
Thirugnanam, H., Ramesh, M.V., Rangan, V.P., 2020. Enhancing the reliability of landslide early warning systems by machine learning. Landslides 17 (9), 2231–2246. https://doi.org/10.1007/s10346-020-01453-z.
Wang, H., Zhang, L., Yin, K., Luo, H., Li, J., 2021. Landslide identification using machine learning. Geosci. Front. 12 (1), 351–364. https://doi.org/10.1016/j.gsf.2020.02.012.
Wen, D., Huang, X., Bovolo, F., Li, J., Ke, X., Zhang, A., Benediktsson, J.A., 2021. Change detection from very-high-spatial-resolution optical remote sensing images: Methods, applications, and future directions. IEEE Geoscience and Remote Sensing Magazine 9 (4), 68–101. https://doi.org/10.1109/MGRS.2021.3063465.
Xia, J., Liu, H., Zhu, L., 2022. Landslide hazard identification based on deep learning and sentinel-2 remote sensing imagery. J. Phys. Conf. 2258 (1), 012031. https://doi.org/10.1088/1742-6596/2258/1/012031. IOP Publishing.
Xu, H., He, H., Zhang, Y., Ma, L., Li, J., 2023. A comparative study of loss functions for road segmentation in remotely sensed road datasets. Int. J. Appl. Earth Obs. Geoinf. 116, 103159. https://doi.org/10.1016/j.jag.2022.103159.

Xu, Y., Ouyang, C., Xu, Q., Wang, D., Zhao, B., Luo, Y., 2024. CAS landslide dataset: a large-scale and multisensor dataset for deep learning-based landslide detection. Sci. Data 11 (1), 12. https://doi.org/10.1038/s41597-023-02847-z.

Yang, S., Wang, Y., Wang, P., Mu, J., Jiao, S., Zhao, X., Wang, Z., Wang, K., Zhu, Y., 2022. Automatic identification of landslides based on deep learning. Appl. Sci. 12 (16), 8153.

Yi, Y., Xu, X., Xu, G., Gao, H., 2023. Landslide detection using time-series InSAR method along the Kangding-Batang section of Shanghai-Nyalam road. Rem. Sens. 15 (5), 1452.

Zhang, M., Chen, F., Liang, D., Tian, B., Yang, A., 2020. Use of Sentinel-1 GRD SAR images to delineate flood extent in Pakistan. Sustainability 12 (14), 5784. https://doi.org/10.3390/su12145784.

Zhang, Q., Wang, T., 2024. Deep learning for exploring landslides with remote sensing and geo-environmental data: frameworks, progress, challenges, and opportunities. Rem. Sens. 16 (8), 1344–1347.

Zhang, S., Li, R., Wang, F., Iio, A., 2019. Characteristics of landslides triggered by the 2018 hokkaido eastern Iburi earthquake, northern Japan. Landslides 16, 1691–1708. https://doi.org/10.1007/s10346-019-01207-6.